



SWAMP: A new experiment for simulating permafrost warming and active layer deepening on the Tibetan Plateau

Yuxuan Bai¹ | Yunfeng Peng¹ | Wei Zhou^{1,2} | Yuhong Xie^{1,2} | Qinlu Li^{1,2} | Guibiao Yang¹ | Leiyi Chen¹ | Biao Zhu³ | Yuanhe Yang^{1,2}

¹State Key Laboratory of Vegetation and Environmental Change, Institute of Botany, Chinese Academy of Sciences, Beijing, China

²University of Chinese Academy of Sciences, Beijing, China

³Institute of Ecology, College of Urban and Environmental Sciences, and Key Laboratory for Earth Surface Processes of the Ministry of Education, Peking University, Beijing, China

Correspondence
 Yuanhe Yang
 Email: yhyang@ibcas.ac.cn

Funding information
 National Key Research and Development Program of China, Grant/Award Number: 2022YFF0801902; National Natural Science Foundation of China, Grant/Award Number: 31988102, 31825006, 32201405 and 32241034

Handling Editor: Jessica Royles

Abstract

- Our knowledge on the responses of permafrost ecosystems to climate warming is critical for assessing the direction and magnitude of permafrost carbon-climate feedback. However, most of the previous experiments have only been able to warm the air and surface soil, with limited effects on the permafrost temperature. Consequently, it remains challenging to realistically simulate permafrost thawing in terms of increased active layer (a layer freezing and thawing seasonally above permafrost) thickness under climate warming scenarios.
- Here, we presented the experimental design and warming performance of a novel experiment, Simulate Warming at Mountain Permafrost (SWAMP), the first one to successfully simulate permafrost warming and the subsequent active layer deepening in a swamp meadow situated on the Tibetan Plateau. Infrared heating was employed as above-ground warming to elevate the temperature of the air and surface soil, and heating rods were inserted vertically in the soil to provide below-ground warming for transmitting heat to the deep active layer and even to permafrost deposits.
- In 3 m diameter warmed circular plots, the air and the entire soil profile (from surface soil to 120 cm) was effectively heated, with an increase of approximately 2°C in the upper 60 cm, which progressively weakened with soil depth. Warming increased soil moisture across the growing season by inducing an earlier thawing of the soil. Values varied from 1.8 ± 1.8 to $12.3 \pm 2.3\%$ according to the soil depth. Moreover, during the growing season, the warmed plots had greater thaw depths and a deeper active layer thickness of 12.6 ± 0.8 cm. In addition, soil thawing duration was prolonged by the warming, ranging from 22.8 ± 3.3 to 49.3 ± 4.5 days depending on the soil depth.
- The establishment of SWAMP provides a more realistic simulation of warming-induced permafrost thaw, which can then be used to explore the effect of climate warming on permafrost ecosystems and the potential permafrost carbon-climate feedback. Notably, our experiment is more advantageous for investigating how

Revised manuscript submitted to Methods in Ecology and Evolution.

This is an open access article under the terms of the [Creative Commons Attribution](#) License, which permits use, distribution and reproduction in any medium, provided the original work is properly cited.

© 2023 The Authors. *Methods in Ecology and Evolution* published by John Wiley & Sons Ltd on behalf of British Ecological Society.

deep soil processes respond to climate warming and active layer deepening, compare with experiments which use passive warming techniques such as open top chambers (OTCs).

KEY WORDS

active layer thickness, active warming technique, carbon cycle, climate change, deep soil warming, permafrost, whole-ecosystem warming

1 | INTRODUCTION

Permafrost (ground that keeps frozen at or below 0°C for two or more consecutive years; Permafrost Subcommittee, 1988) covers about $2.3 \times 10^7 \text{ km}^2$, accounting for 16% of the global land area (Zhang et al., 2008). In the Northern Hemisphere, permafrost is primarily found at high-latitude region, for example Alaska and Siberia, and in high-altitude areas, for example the Tibetan Plateau (Obu et al., 2019). In these regions, microbial decomposition is limited due to the prolonged low temperature and freezing conditions, which in turn leads to an accumulation of soil organic carbon (SOC; Johnston et al., 2019). The soil carbon pool in the top 3 m across permafrost regions has recently been estimated to be 1014 Pg C (1 Pg = 10^{15} g), approximately double the size of the atmospheric carbon pool (Mishra et al., 2021). However, this large carbon pool is currently threatened by continuous climate warming. In particular, permafrost with zero annual amplitude (the depth at which the yearly fluctuations in temperature fall below 0.1°C; French & Shur, 2010) has experienced a significant climate warming of 0.29°C over the last decade (Biskaborn et al., 2019). The rise in temperature accelerates permafrost thaw, resulting in an increase in active layer thickness (e.g. 0.15 cm per year in the Arctic and 1.95 cm per year on the Tibetan Plateau; Wang et al., 2022) and abrupt permafrost thaw (e.g. the formation of thermokarst landscape features such as thermokarst lake; Olefeldt et al., 2016). These changes in the thermal state of permafrost deposits may leave more SOC available for microbial decomposition, subsequently release significant quantities of greenhouse gases [e.g. carbon dioxide (CO_2) and methane (CH_4)], and potentially create a positive feedback between permafrost carbon and climate warming (Johnston et al., 2019; Miner et al., 2022; Schuur et al., 2015). However, there is considerable variation in model prediction of changes in permafrost carbon under the impacts of climate change [ranging from -641 to 167 Pg C under Representative Concentration Pathway (RCP) 8.5, the highest baseline emission scenario throughout the 21st century; McGuire et al., 2018]. To minimize these uncertainties, various approaches have been used such as *in situ* warming experiments (Henry & Molau, 1997), observations across temperature gradients (Hugelius & Kuhry, 2009), and laboratory incubation (Chen et al., 2016). Manipulative warming experiments have an important place among these approaches since they overcome most of the limitations of gradient and laboratory studies (Torn et al., 2015). Therefore, synchronous *in situ* simulations of permafrost warming and the subsequent active layer deepening can

greatly contribute to a comprehensive understanding of permafrost carbon-climate feedback, especially regarding the direction and magnitude of the feedback.

During the past several decades, great efforts have been made to better understand the responses of permafrost ecosystems to climate warming with multiple *in situ* manipulative experiments (Henry & Molau, 1997; Natali et al., 2011). The best known of these is the International Tundra Experiment (ITEX), established in the Arctic tundra in 1990. Using open top chambers (OTCs) to simulate warming, ITEX explored the phenology, growth and functional traits of vascular plants in response to climate warming (Henry & Molau, 1997). Although OTCs are effective in warming air and surface soil, the warming effects on deep soil (e.g. >50 cm) and permafrost are very limited (Marion et al., 1997), which constrains our understanding of the responses of deep soil carbon dynamics to permafrost thaw. With this limitation in mind, the Carbon in Permafrost Experimental Heating Research (CiPEHR) combined both ITEX-style OTCs and snow fences to make successful strides in simulating deep soil warming and active layer deepening in Alaska (Natali et al., 2011). These passive warming techniques are effective in permafrost regions where the active layer is shallow (e.g. ~50 cm in the Arctic; Luo et al., 2016), but their effects may be inadequate when the active layer is thick (e.g. more than 100 cm on the Tibetan Plateau; Wang et al., 2022). Therefore, there is an urgent need to develop a novel approach to achieve ecosystem warming in permafrost regions with a thick active layer, that is simulation of both air and soil warming, as well as active layer deepening.

The development of next-generation whole-soil-profile and whole-ecosystem warming technologies offers a great opportunity to simulate permafrost thawing, and in particular, the increase in active layer thickness. These approaches utilize active warming techniques to simultaneously elevate the temperature of the air and the entire soil profile (Hanson et al., 2011). Using these technologies, deep soil temperature (e.g. 1–2 m) has been increased by 4–9°C (Hanson et al., 2017; Hicks Pries et al., 2017; Nottingham et al., 2020; Qin et al., 2023). The development of such technologies aims to establish a more realistic scenario of future ecosystem change to explore the responses of ecosystem structure and function to climate change and the mechanisms involved (Torn et al., 2015). For permafrost ecosystems, the response of deep soil processes to active layer deepening is particularly important because deep SOC may be more vulnerable to global warming, and consequently have profound impacts on the ecosystem carbon balance (Koven et al., 2015). As yet, however, there are no reports of the application of these

technologies, or modified versions, in permafrost ecosystems, and our understanding of the deep soil processes in response to permafrost thaw remains constrained by experimental limitation.

Here, we introduce a novel warming experiment, Simulate Warming at Mountain Permafrost (SWAMP), established in 2021 in a swamp meadow on the Tibetan Plateau. Combining the concepts of whole-soil-profile and whole-ecosystem warming, SWAMP implemented a redesigned warming system that effectively simulates the increase in permafrost temperature during the growing season, as well as active layer deepening. Infrared heaters were used to warm the air and the surface soil, and heating rods being inserted vertically in the soil were employed to transmit heat into the deep soil and, in particular, into permafrost deposits. To characterize the warming effects of SWAMP, measurements of the temperature of the air and the whole soil profile (from surface soil to permafrost table) and soil moisture at various depths were taken for a full year. In addition, warming effects on thawing depths and thawing duration at different depths of the active layer were also recorded from May to October. Here, our main objective is to present the experimental design and warming performance of this first whole-ecosystem warming experiment in permafrost regions, which simulates air and soil warming and active layer deepening utilizing active warming technique. With this unique experiment, we seek to provide a more realistic scenario for the impacts of future climate warming on permafrost ecosystems and to shed more insights on how these ecosystems, and in particular their deep soil carbon dynamics, will respond to climate warming and subsequent permafrost thaw.

2 | MATERIALS AND METHODS

2.1 | Study region and site description

The Tibetan Plateau hosts $1.1 \times 10^6 \text{ km}^2$ of high-altitude permafrost (the largest area in the world at low or middle latitudes), which accounts for 40.2% of the region (Cheng et al., 2019). The mean annual air temperature and precipitation in this area range from -4.9 to 6.1°C and 84.3 to 593.9 mm , respectively (Ding et al., 2016). The plateau contains a variety of alpine ecosystems, including alpine forest, shrubland, meadow, steppe and desert, with grassland ecosystems predominating (Zhang et al., 1988). Large amounts of SOC are stored in this alpine permafrost region, with the soil carbon stock in the upper 3 m being estimated at 15.3 – 21.7 Pg C (Ding et al., 2016; Wang, Wu, et al., 2021). Over the past three decades, the plateau has experienced considerable climate warming, with an average change in air temperature ($\sim 0.5^\circ\text{C}$ per decade; Kuang & Jiao, 2016) of approximately twice the rate of global warming over the same period (Cheng et al., 2019). The soil temperature in active layer and permafrost has also increased during this period (0.3 – 0.5°C per decade for the active layer of 0 – 40 cm [see also Figures S1] and 0.02 – 0.3°C per decade for permafrost at 10 m depth; Wu & Zhang, 2008). Under the impact of soil warming, the active layer thickness has been increasing at a rate of 5 – 20 cm per decade over the last three decades (Peng et al., 2018; Wang et al., 2022). Current measurements of the active layer

thickness in the Tibetan alpine permafrost region give values about 100 – 320 cm (Xu & Wu, 2021). Under future climate change scenarios, the active layer thickness of this alpine permafrost region is predicted to increase at a rate of 6 – 8 cm per decade (Shared Socioeconomic Pathways [SSP] 245; the scenario with a medium pathway for future greenhouse gas emissions) and 18 – 33 cm per decade (SSP 585; the scenario of the upper boundary of greenhouse gas emissions) towards to the end of this century (Xu & Wu, 2021; Zhang et al., 2022).

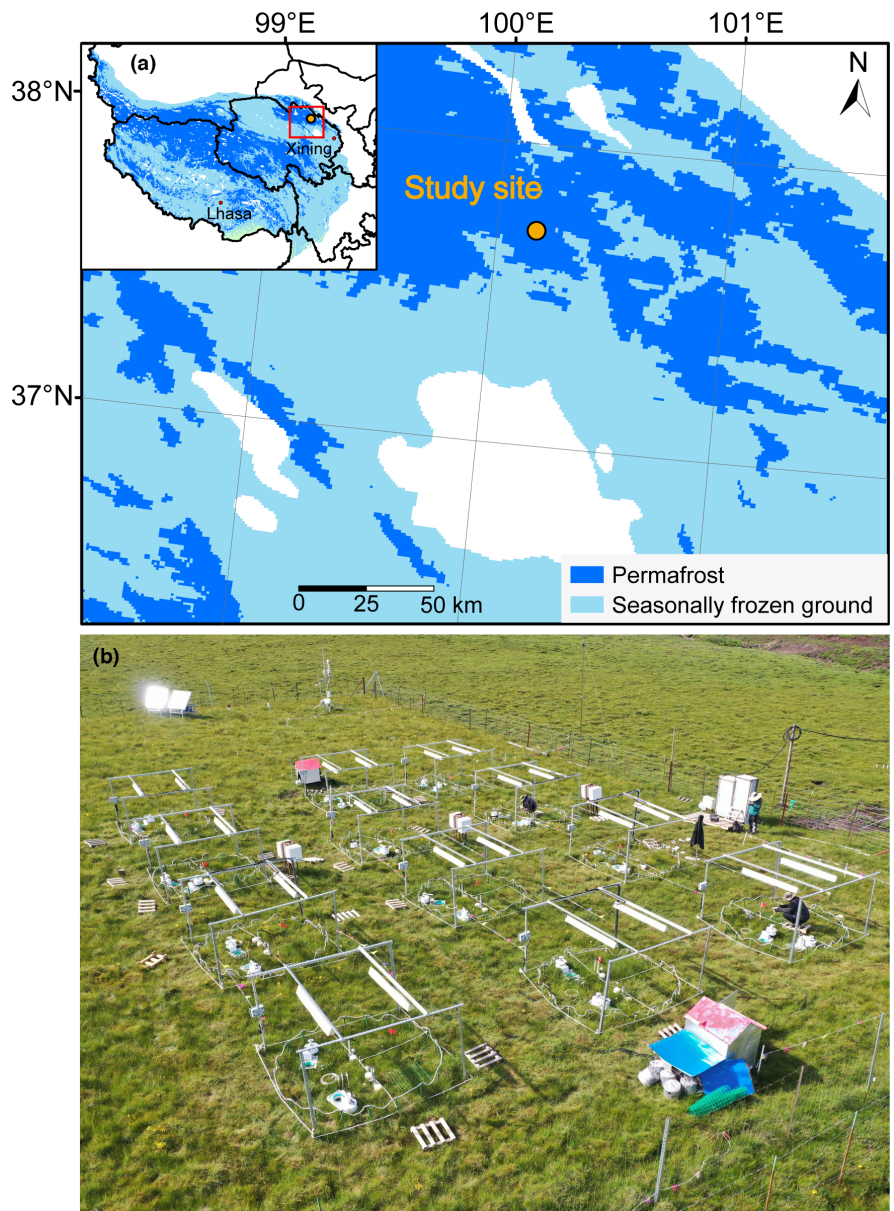
The SWAMP experiment is located in the east of the Altun-Qilian Mountain ranges (37.50°N , 100.24°E ; elevation: 3670 m a.s.l.; Figure 1a), in one of the five typical permafrost regions on the Tibetan Plateau (Jin et al., 2011). The site is characterized by a highland continental climate, with a warm, humid summer and a cold, dry winter (Li et al., 2020). The mean annual temperature during 1959–2020 was -0.1°C , and varied at the rate of 0.3°C per decade over this period (Figure S3). The mean monthly air temperature in the study area fluctuates from a minimum of -13.3°C in January to a maximum of 11.2°C in July (data from the National Meteorological Information Center of China). Mean annual precipitation during 1959–2020 was 364.6 mm , of which approximately 92% fell between May and September (data from the National Meteorological Information Center of China). The experiment site is located within a sporadic permafrost area with the active layer thickness of 120 cm (Li et al., 2022). Permission for fieldwork is non-required.

The vegetation at the site is swamp meadow, one of the three dominant grassland types on the Tibetan Plateau (alpine steppe, alpine meadow and swamp meadow) and the one with the highest SOC density (carbon amount per area) and soil moisture (Ding et al., 2016). The plant community is dominated by sedge, including *Carex tibetikobresia*, *Carex kowanica* and *Carex atrofusca*, with these three species making up nearly 78% of the community cover. Other vascular plants at the site are *Triglochin maritima*, *Carex scabirostris* and *Pedicularis longiflora* etc. (Table S1). Vegetation coverage is approximately 100%, with species richness of $11.2 \pm 0.8 \text{ m}^{-2}$ (this and subsequent data are given as mean \pm SE) and above-ground biomass of $210.0 \pm 13.0 \text{ g m}^{-2}$. The soil is classified by the FAO system as Cambisols (Li et al., 2020). The carbon and nutrient content of the surface soil (0 – 10 cm) is extremely high, with a SOC content of $209.6 \pm 2.8 \text{ mg g}^{-1}$, total nitrogen content of $16.2 \pm 0.2 \text{ mg g}^{-1}$ and dissolved inorganic nitrogen (DIN) of $21.6 \pm 1.7 \text{ mg kg}^{-1}$. The pH is 6.4 ± 0.1 , a value associated with a low content of soil inorganic carbon ($0.28 \pm 0.03 \text{ mg g}^{-1}$). Soil carbon, nutrient and other physicochemical properties are not significantly different between the plots selected for control and warming at any depth (Figures S4–S6 and Table S3), indicating little spatial heterogeneity within the experimental area. DIN content in deep soil was comparable to that in surface soil (Figure S5), in line with the observed patterns in the Arctic (Beermann et al., 2017; Salmon et al., 2018).

2.2 | Experimental design

The SWAMP experiment was established in May 2021. The experimental area was fenced to avoid anthropogenic disturbance, and the

FIGURE 1 Location and the active view of the SWAMP experiment. Geographical location of the study site (a) and the aerial view of the warming experiment plots (b). The permafrost map is derived from Zou et al. (2017). Photograph in panel (b) was taken by W. Zhou in August 2021.



experimental plots were set on gently sloping terrain within a 50×50m area (Figure 1b). The experiment was a paired design that consisted of six replicated blocks to eliminate the influence of topography and the microenvironment. Each replicate block contained two treatments: control and warming. Each experimental plot was a circle of 3m in diameter with an area of approximately 7.1m², and a buffer zone of ~3m was set up between plots to avoid the impact of neighbouring plots. In total, the experimental area occupied approximately 600m² (Figure 2a).

2.3 | Warming system

Infrared heater (Kimball, 2005) was used for above-ground warming, while heating rods inserted vertically into the soil (Hanson et al., 2011) provided below-ground warming (Figure 3). The experiment was set up to actively increase the temperature of the air and the soil (from the active layer to permafrost). The warming

magnitude was set at 2°C since the air and soil temperature of global permafrost is predicted to be increase by ~2°C under the RCP 4.5 scenario (an intermediate baseline emission scenario throughout the 21st century; Soong et al., 2020), and the rise in air temperature on the Tibetan Plateau is also predicted to be raise ~2°C under the RCP 4.5 scenario by the end of this century compared to 2020 (Zhang et al., 2022).

Above the ground, two infrared heaters (8mm diameter×151cm long, 2000W, 240V Model, HS-2420, Kalglo Electronics, USA) were suspended parallel at a height of 1.5 m above the ground to provide as homogeneous a warming as possible without overheating of the vegetation (Kimball et al., 2018). When the above-ground warming system was in operation, the infrared heaters emitted radiation that warmed the air and surface soil. For the below-ground part, 21 heating rods (20 around the perimeter of the circular experimental plot at equal spacing and one in the center; steel tube) were vertically installed into the soil

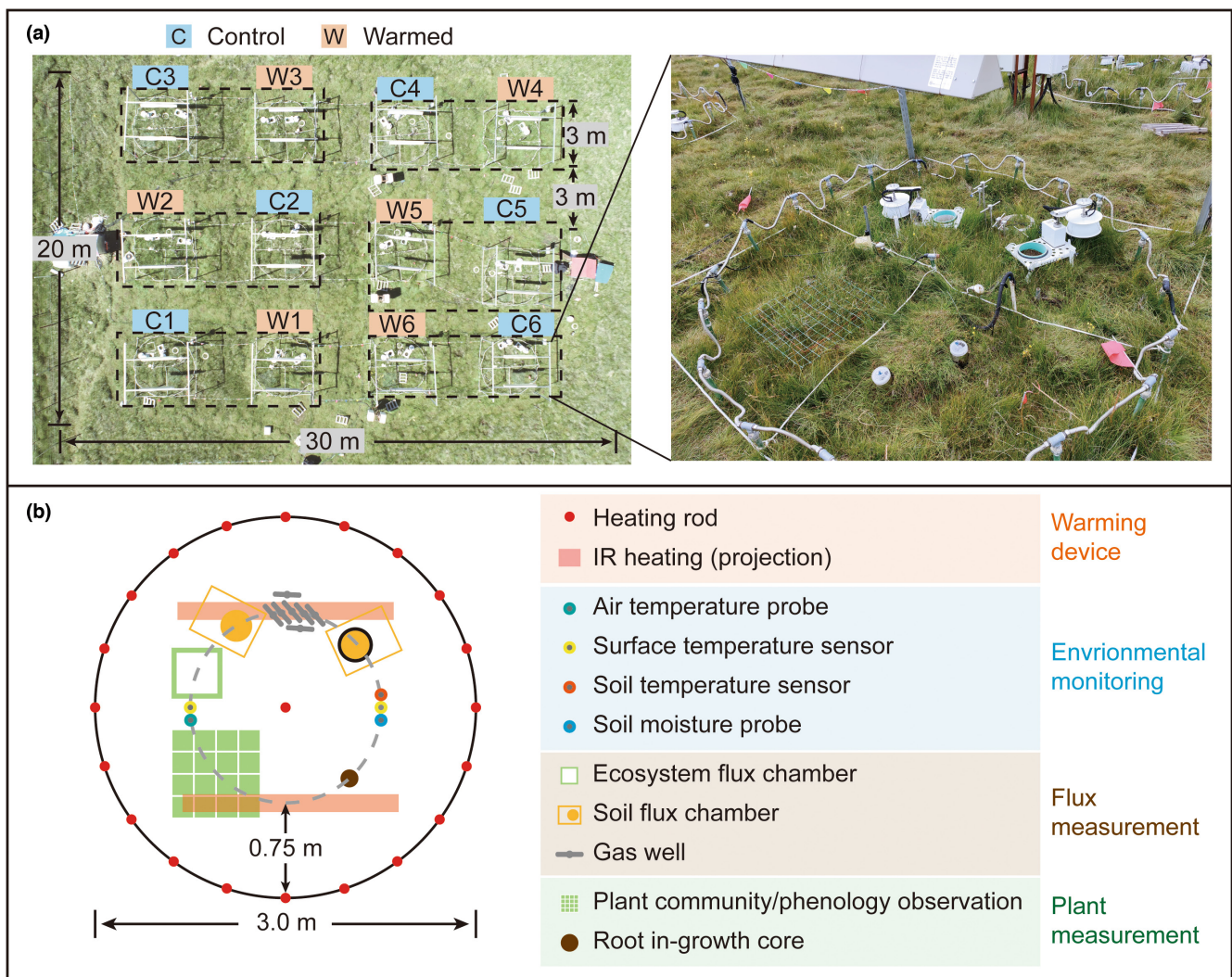


FIGURE 2 The design of the SWAMP experiment. The experiment was a paired design with 6 replicates, each plot being a circle of 3 m in diameter (a). Infrared heaters were used for above-ground warming and heating rods were employed for below-ground warming. The layout of measuring devices, including environmental factor, flux and plant measurements (b). Photographs in panel (a) were taken by Y. Bai in July 2022.

(Figure 2b). Heating cables (10 mm width, 33 W m^{-1} , 240 V Mode, BSX 10-2-FOJ, Thermon, USA) were inserted into each heating rod, with the surrounding void filled with quartz sand to hold the heating cable in place and enhance the efficiency of heat transfer (Hanson et al., 2011). In each heating rod, the heating cables were 80 cm long overall, with 60 cm being buried in the soil and remaining 20 cm being exposed above the ground.

The above- and below-ground warming systems were controlled by separate devices, but the workflows were almost identical. In general, the temperature data were first collected using a data logger; secondly, the temperature difference between the warmed and control plots within each pair of treatments was calculated via the computation module; and thirdly, the warming devices were governed based on the temperature difference between the warmed and control plots (Figure 3). Specifically, for the above-ground warming system, two thermocouple

probes (WZP-231, Xincheng Electric Appliance, China; Range: $-50\text{--}250^\circ\text{C}$; Accuracy: $\pm 0.3^\circ\text{C}$) were installed in the surface soil (0–5 cm) and acted as temperature sensors to control the infrared heaters. These two temperature sensors were arranged parallel to the infrared heaters, and were placed equidistant from the centre and edge of the plot (Figures 2b and 3). Temperature data from the two sensors were collected and the difference was calculated by the computation module (Current/Power Output Module, Haiwell Happy, China). The infrared heaters were activated when the average temperature of the two sensors in the warmed plot was less than 2°C warmer than those in the paired control plot. They were turned off when the temperature difference exceeded 2°C . For the below-ground warming system, T-type thermocouples (TX-FFRP, Shanghai Kaixin Sensor Technology, China; Range: $-40\text{--}200^\circ\text{C}$; Accuracy: $\pm 0.3^\circ\text{C}$) were inserted in a cavity positioned adjacent to one of the above-ground temperature sensors at seven soil depths

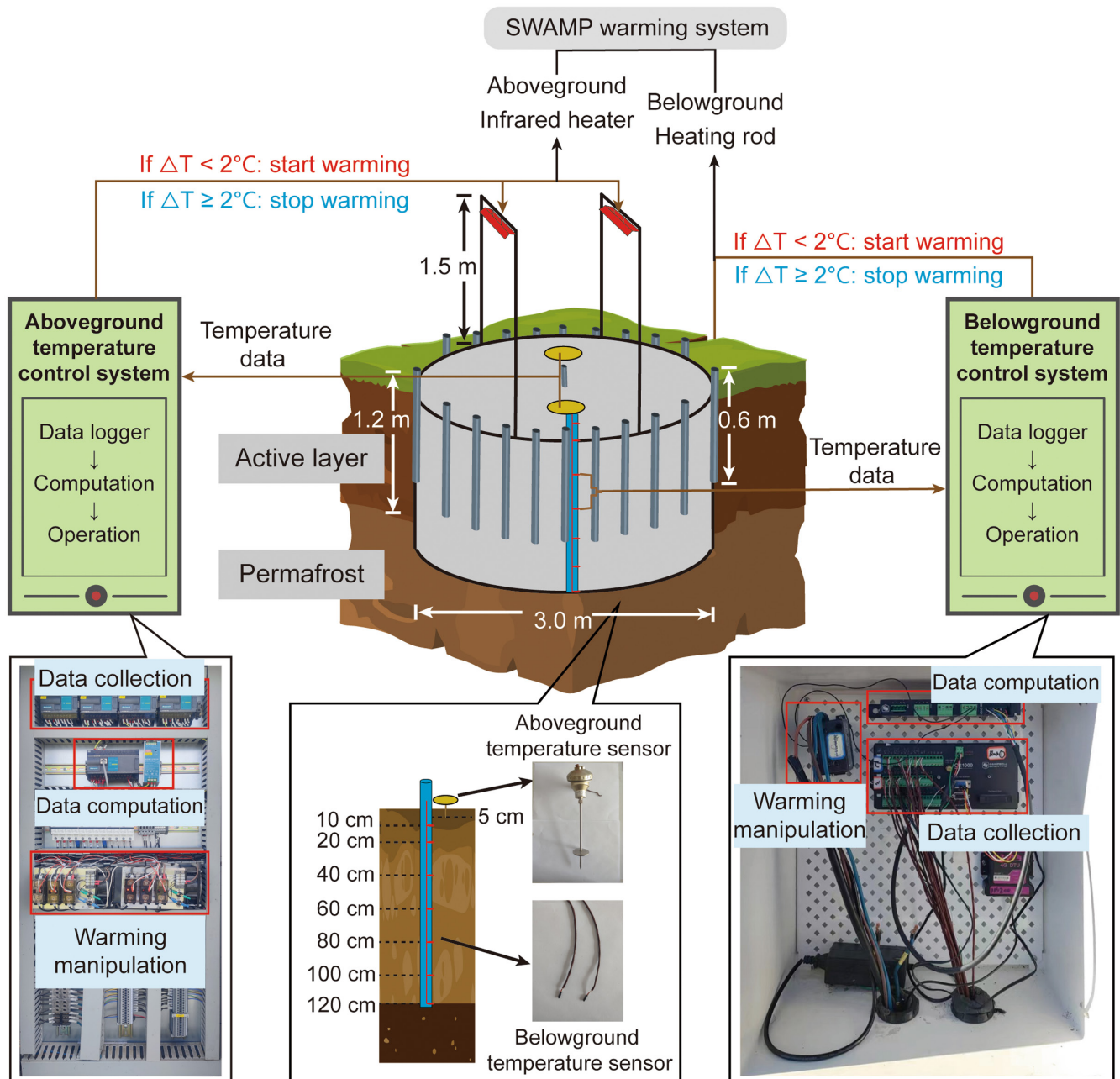


FIGURE 3 Schematic diagram of the operating rules for above- and below-ground warming systems. Workflow: firstly, temperature data were collected using a data logger; secondly, the difference in temperature (warmed-control; ΔT) was calculated; thirdly, warming devices started warming when the temperature difference was less than 2°C , and stopped warming when the temperature difference was higher than 2°C . Two temperature sensors controlling infrared heaters were arranged parallel to the infrared heaters, and were placed equidistant from the centre and edge of the plot (yellow ellipse). Below-ground temperature sensors were inserted in a hole adjacent to one of the above-ground temperature sensors. The location of the temperature sensors is shown in Figure 2b.

(10, 20, 40, 60, 80, 100 and 120 cm [from surface soil to the permafrost table]). Data from these sensors were collected by a data logger (CR1000, Campbell Scientific). When the average value at 40 and 60 cm in the warmed plot was less than 2°C warmer than those in the paired control plot, the heating rods were turned on. When the temperature difference was greater than 2°C , they were turned off (Figure 3). Dummy warming devices were installed in the control treatments (Figure 2a).

2.4 | Warming duration

To mimic the impacts of climate warming and the associated increase in active layer thickness, SWAMP simulated the increase in temperatures of air, active layer and permafrost during the growing season (May–September). For a variety of reasons, warming actions were not undertaken outside of the growing season. First, soil warming in winter kept the active layer from freezing (soil temperature $> 0^\circ\text{C}$;

Figure S8). In fact, under the current scenario, the active layer stays frozen in winter without taliks at our study site (soil temperature $<0^{\circ}\text{C}$; **Figure S8**), so winter soil warming would result in an excessive and unrealistic warming scenario. Second, the primary aim of this experiment was to simulate an increase in active layer thickness, and the thawing process occurs mainly during the growing season. In 2021, the warming system was first turned on in late April (27th April) and its trial run ended in late August (29th August), having been running for a total of 124 days. During this time, the warming system procedures and equipment were constantly tested and adjusted. Based on the main objective of our experiment (i.e. to simulate the increase in active layer thickness), the second-year of warming was initiated on 27th April, 2022, when the active layer began to thaw, and ended, after 160 days, on 4th October, when the active layer began to freeze.

2.5 | Environmental monitoring

Air temperature, soil temperature and soil moisture were recorded continuously in each plot to monitor the effects of the experimental warming on environmental factors. An air temperature probe (DS1923 iButtons, Maxim Integrated) was placed at 10 cm above the ground in each plot. For soil temperature, the sensors of the warming system were employed as measurement devices, and were inserted in one hole into eight depths (from surface soil to the permafrost table at 120 cm). Considering the high water table and prolonged flooding of the deep soil during the growing season at our experimental site (Li et al., 2022), as well as the fact that the experimental plots would be damaged if the soil moisture probes were buried too deeply, soil volumetric moisture was measured at four depths (10, 20, 40 and 60 cm; 5TM-EM50, Decagon). All data were recorded at 1-hour intervals. Altogether, each experimental plot contained one air temperature probe, and eight soil temperature probes as well as four soil moisture probes at different depths (**Figure 2b**). Thawing depth was measured using a thaw-probe three times a month from May to October, that is during the period of active layer thawing. Four measurement points were selected equally in a line from the centre to the edge of each plot to determine the thawing depth of the active layer (Natali et al., 2011). To determine thawing duration (period of nonfreezing), the start time for the thawing period at various depth was measured manually using the thaw-probe, while the end time was taken to be the day when the minimum temperature at or fell below 0°C from that day onwards (Wang et al., 2016).

2.6 | Statistical analyses

First of all, the continuously recorded one-hour data (e.g. air and soil temperature, and soil moisture) were averaged to the daily scale. To evaluate warming effects on air temperature, soil temperature and soil moisture at each depth, we used linear mixed effect models with the warming treatment as a fixed variable, and block nested within

observation date (day) as random factors to account for repeated measurements. Then, to examine the warming effect on maximum thawing depth (i.e. the active layer thickness) and thaw duration at various depths, other linear mixed effect models were applied with warming treatment as a fixed variable, and block as a random variable. In addition, to explore the spatial homogeneity of the experimental plots, we collected soil samples at different depths in each experimental plot before warming (i.e. October, 2020) and measured for soil physicochemical properties (e.g. soil carbon and nitrogen content, moisture and pH; for details about the measurements of these variables, see Appendix S1). We performed linear mixed effect models on soil properties, using treatment division (i.e. warmed and control) and soil depth as fixed variables, and block as a random variable. Data that did not have normally distributed residuals were log- or arcsin-transformed. The *p* value of each linear mixed effect model was adjusted using the ‘Bonferroni’ method (Benjamini & Hochberg, 1995). All statistical analyses were conducted in R v4.1.2 (R Core Team, 2022), and the LME4 and LMERTEST packages were used to perform the linear mixed effect models (Kuznetsova et al., 2017).

3 | RESULTS

Daily air temperature varied seasonally, ranging from $-13.7 \pm 0.9^{\circ}\text{C}$ (this and subsequent results are given as mean \pm SE) in January and $16.2 \pm 0.2^{\circ}\text{C}$ in August in the control plots (**Figure 4a**). Soil temperatures also exhibited a strong seasonal variation, with the lowest temperatures in the non-growing season (0–100 cm in February and 120 cm in March) and the highest in growing season (0–60 cm in August, 80–120 cm in September), but the differences between seasons decreased with soil depth (**Figure 5**). During the period when the warming system was operational (from May to September), warming significantly increased the temperature of the air and the soil at different depths (**Figures 4** and **5** and **Table S2**). Specifically, the average air temperature was increased by $1.8 \pm 0.6^{\circ}\text{C}$, from $11.4 \pm 0.1^{\circ}\text{C}$ to $13.3 \pm 0.6^{\circ}\text{C}$ (**Figure 4b**). The soil temperature was increased by the warming by approximately 2°C in the upper 60 cm (**Figure 5a–e**), with increases of $2.1 \pm 0.1^{\circ}\text{C}$ for the surface soil (0–5 cm), $1.8 \pm 0.1^{\circ}\text{C}$ at 10 cm, $1.8 \pm 0.3^{\circ}\text{C}$ at 20 cm, $1.9 \pm 0.3^{\circ}\text{C}$ at 40 cm, and $2.0 \pm 0.4^{\circ}\text{C}$ at 60 cm (**Figure 5i**). Below 60 cm, however, the effect of warming on soil temperature decreased with increasing soil depth (**Figure 5f–h**), with increases of $1.4 \pm 0.1^{\circ}\text{C}$ at 80 cm, $1.1 \pm 0.2^{\circ}\text{C}$ at 100 cm, and $0.6 \pm 0.1^{\circ}\text{C}$ at 120 cm (**Figure 5i**).

Soil volumetric moisture exhibited contrasting seasonal variations to those of soil temperature. During the growing season, soil moisture remained at a high level, with values of $51.1 \pm 1.7\%$ at 10 cm, $47.6 \pm 1.2\%$ at 20 cm, $37.1 \pm 1.4\%$ at 40 cm and $21.4 \pm 1.6\%$ at 60 cm (**Figure 6a–d**). Similar to soil temperature, soil moisture was affected by the warming, but the magnitude varied across soil depths (**Figure 6a–d** and **Table S2**). During the period of experimental warming, warming had a minor effect on soil moisture at 10 cm, increasing it by $1.8 \pm 1.8\%$, from $51.1 \pm 1.7\%$ to $52.9 \pm 1.0\%$ (**Figure 6a**). The effect of warming on soil moisture grew gradually with soil depth, with

FIGURE 4 Daily mean (\pm SE, $n=6$) air temperature in warmed and control treatments across the year of 2022 (a), and the total mean air temperature in warmed and control treatments and the difference (warmed – control; mean \pm SE, $n=6$) of air temperature during the growing season (May–September) in 2022 (b). The grey background in panel (a) represents the period of warming treatment. Significant level: ***, $p < 0.001$. Detailed statistical results can be seen in Table S2.

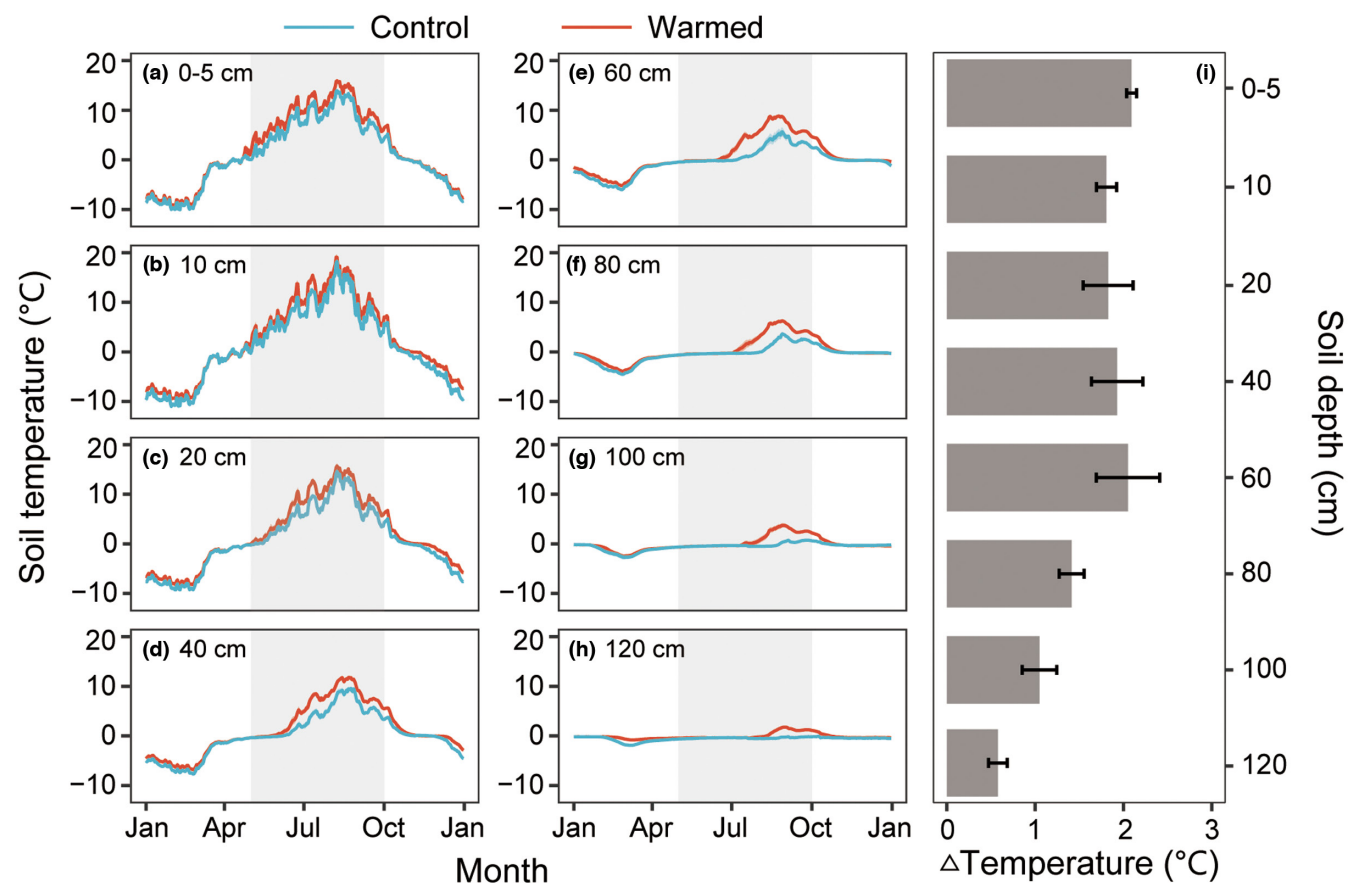
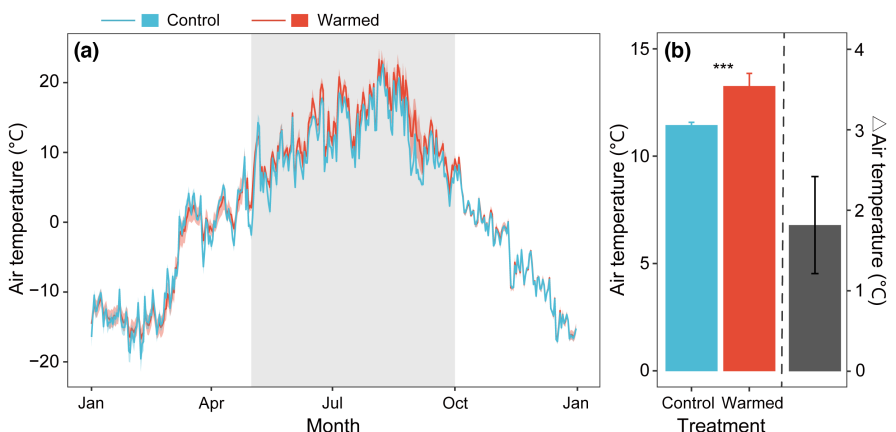


FIGURE 5 Daily mean (\pm SE, $n=6$) temperature in warmed and control treatments from surface soil (0–5 cm) to deep soil (120 cm) across the year of 2022 (a–h), and the mean differences (\pm SE, $n=6$; warmed–control) in soil temperature at different depths along the soil profile during the growing season (May–September; i) in 2022. The grey background in panels (a–h) represents the period of warming treatment. Detailed statistical results are given in Table S2.

soil moisture increasing by $4.3 \pm 2.1\%$ at 20 cm, $6.0 \pm 3.4\%$ at 40 cm, and $12.3 \pm 2.3\%$ at 60 cm (Figure 6e).

The thawing period of the active layer began in May and was completed in early October. Warming accelerated the active layer thawing, and thawed the permafrost (Figure 7). The thawing depth in the warmed plots was significantly greater than that in the control plots throughout the growing season (Figure 7a). The largest

difference in thawing depth occurred in August (33.2 ± 2.4 cm), an increase of 37.6% compared to the control (Figure 7a). The active layer thickness was also promoted by warming, with an increase of 10.5% occurring in early October (control: 120.0 ± 1.4 cm; warmed: 132.6 ± 0.8 cm; increase of 12.6 ± 0.8 cm; Figure 7b). Thawing duration throughout the soil profile was significantly prolonged by warming (Figure 7c). The effect of warming on thawing duration

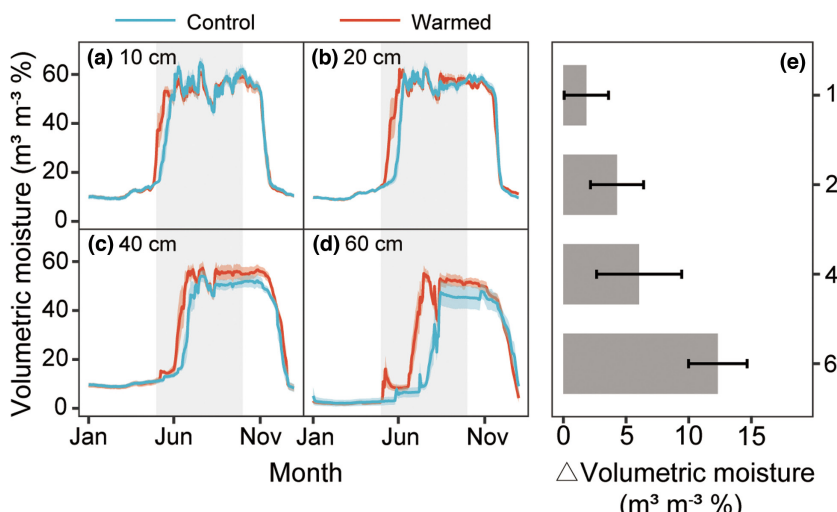


FIGURE 6 Daily mean (\pm SE, $n=6$) soil volumetric moisture in warmed and control treatments from 10 to 60 cm across the year of 2022 (a–d), and the mean differences (\pm SE, $n=6$; warmed–control) in soil volumetric moisture at different depths along the soil profile during the growing season (May–September) in 2022 (e). The grey background in panels (a–d) represents the period of warming treatment. Detailed statistical results are given in Table S2.

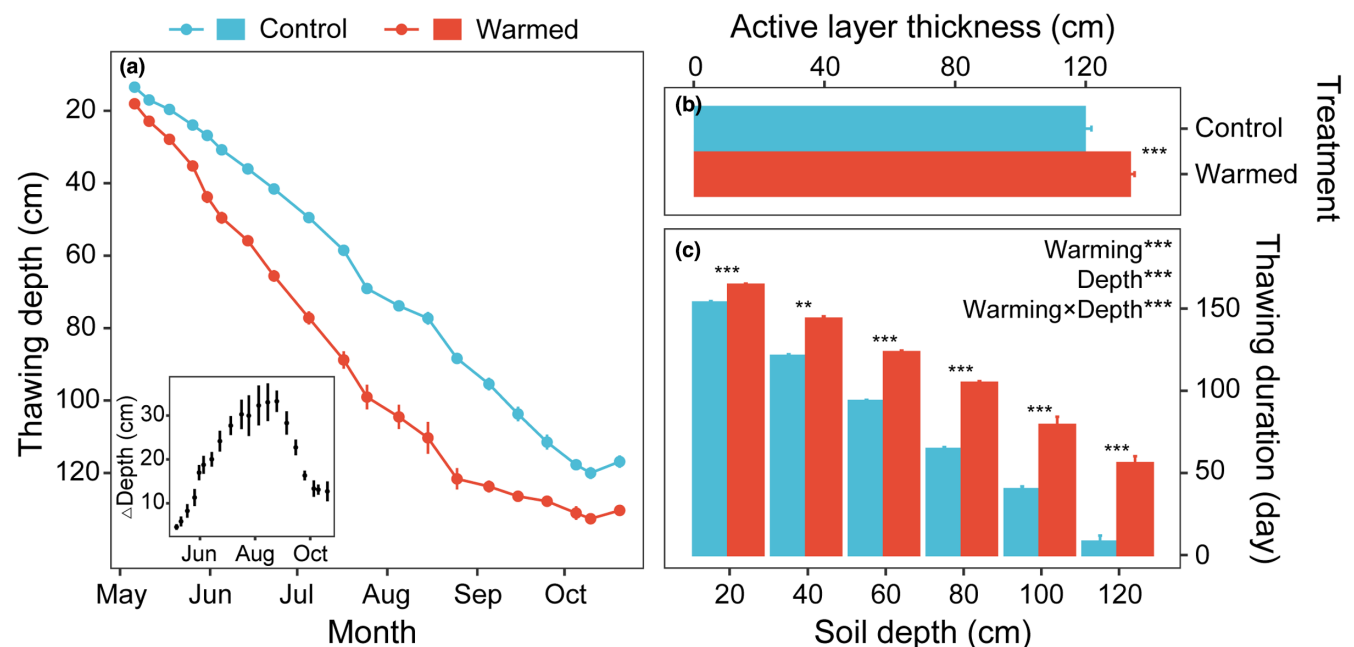


FIGURE 7 Thawing depth (mean \pm SE, $n=6$; a) and thickness (mean \pm SE, $n=6$; b) of the active layer in control and warmed treatments. The lower left figure in panel (a) represents the differences in thawing depth (warmed–control; Δ depth) from May to October of 2022. Thawing duration at different soil depths in the control and warmed treatments in 2022 (c). The start time of the thawing period at various soil depths was determined manually using the thaw-probe, and the end time was specified as the day on which the minimum temperature at or below 0°C from that day onwards (Wang et al., 2016). Detailed statistical results are given in Table S2. Significant level: ***, $p < 0.001$.

gradually increased with soil depth (Table S2), with the smallest increase of 22.8 ± 3.3 days occurring at 20 cm, and the largest increase of 49.3 ± 4.5 days at 120 cm.

4 | DISCUSSION

Our results showed that soil temperature was steadily elevated by 2°C in the upper 60 cm (Figure 5). This warming effect was comparable to the effect of whole-soil-profile warming, consistently increasing the soil temperature to a target warming within the insertion depth of the heating rods (Hanson et al., 2011). However, for

the whole-soil-warming experiments, the increase in temperature of the surface soil was significantly lower than the increases in the subsoil. This is probably due to heat dissipation from the surface soil being greater than the heat supply from the heating rods (Hicks Pries et al., 2017; Nottingham et al., 2020; Qin et al., 2023). By combining infrared heaters with the heating rods to compensate for the insufficient warmth of the surface soil, the current experiment overcame this shortcoming and achieved almost the same magnitude of warming in the surface soil as in the subsoil. Moreover, below 60 cm, the magnitude of soil warming gradually decreased (Figure 5). This pattern was largely in line with long-term observations in the Tibetan alpine permafrost region (Hu et al., 2019; see also Figures S1). In this

region, soil temperature variations in the upper layers were almost identical (increased by 0.44–0.45°C per decade in the upper 40 cm), but they weakened with increasing soil depth (0.24–0.40°C per decade from 40 to 200 cm) during the last few decades (Figure S2). In the current experiment, the increase in soil temperature below 60 cm was mainly induced by heat transfer from upper layers, rather than by direct heating of the soil column as occurred in the upper 60 cm. In fact, the soil warming rate has also declined with soil depth in the Tibetan alpine permafrost region during the last few decades (Liu et al., 2017; Zhang et al., 2020). According to data obtained from permafrost boreholes in this region, the warming rate of the active layer (~0.2°C per decade) was roughly twice that of the permafrost layer (0.09–0.12°C per decade; Zhang et al., 2020). This temporal variation in soil temperature with depth in cold regions seems to be less consistent than the trend in warm regions, that is temperature increases were similar at the surface and at the depths (Soong et al., 2020). The difference is possibly because deep soils in this region may have a greater specific heat capacity due to their higher water content (Yadav & Saxena, 1973), and more of the heat intake from climate warming may become latent heat rather than sensible heat (Halliwell & Rouse, 1987). Our SWAMP experiment therefore provides a relatively realistic simulation of changes in the soil temperature under the influence of climate change in the Tibetan alpine permafrost region, that is relatively consistent trends in the upper layers and a gradual decrease in the deeper layers.

The insertion depth of the heating rods determines the extent and degree of heat transfer (Hanson et al., 2011). Before the start of our warming experiment, many attempts had been made to determine an appropriate insertion depth for the heating rods by comparing the warming effects of insertion into permafrost (more than 120 cm), 80, 60 and 40 cm (More details were given in Appendix S2). When the heating rods were inserted into the permafrost, warming induced rapid permafrost degradation and collapse of the ground, creating a landscape similar to that of thermokarst lakes (Figure S9a–c). Although our study site has experienced significant climatic warming over the last few decades, the prevalent form of permafrost thawing has been active layer deepening (Zhang et al., 2022). As the climate gets warmer, thermokarst landscapes might form; however, in the current period, we aim to first simulate the increase in active layer thickness. Within the next few years, with the accumulation of heat, it is anticipated that thermokarst landscapes can be simulated. By comparing the effects of insertion of the heating rods at 40, 60 and 80 cm, we found that the permafrost received only modest warming when heating rods were inserted at 40 cm (Figure S8g,n), while the surface collapsed significantly when they were inserted at 80 cm (Figure S9i). However, the permafrost was warmed appropriately without the surface collapsing rapidly, when the heating rods were inserted at 60 cm (Figures S8g,n and S9h). Therefore, a 60 cm heating rod insertion was ultimately selected to directly warm the active layer in the upper 60 cm, and to transmit heat to the deeper layers down to the permafrost deposits. Such a design allowed for a better simulation of the increase in active layer thickness, which has been reported to occur widely across the Tibetan alpine permafrost region (Xu & Wu, 2021).

Although both this experiment and the whole-soil-profile warming experiments utilized heating rods to elevate soil temperature, the designs of the below-ground warming system were not identical. Rather than the 'multi-loop rod' layout (heating rods arranged in multiple loops within the plot; Hanson et al., 2017; Figure S10a) used in the whole-ecosystem warming or the 'single-loop rod + multi-loop cable' layout (one loop of heating rod with multiple loops of heating cable inside in the plot; Hicks Pries et al., 2017; Qin et al., 2023; Figure S10b) used in the whole-soil-profile warming experiment, we used a 'loop + point rod' layout (Figure S10d). This design consisted of 20 heating rods inserted around the perimeter of the circular plot and one in the centre. Such a '20+1' layout is novel for a below-ground warming system but, according to the results of our experiment, achieved the desired effect. Compare with the 'multi-loop rod' layout for large plots, a central heating rod has a lower energy consumption, higher efficiency for deep soil warming and is more suitable for plots of a relatively small size. In addition to these below-ground differences, the design of the above-ground warming system was also different from that of the current whole-ecosystem warming experiment in a spruce-peatland ecosystem in Minnesota, USA (Spruce and Peatland Responses Under Changing Environments; SPRUCE; Hanson et al., 2017). In contrast to that experiment, we employed an infrared heating technique, which is cheaper and less disruptive than the massive OTC-style chamber, which cannot warm in open-field conditions (Hanson et al., 2017; Kimball et al., 2018). In addition to their use in our trial, infrared heaters have also been used as the above-ground warming devices in other ecosystems where, as in our study, dwarf herbaceous plants predominate in the communities (Liu et al., 2018; Noyce et al., 2019; Xue et al., 2017). In addition, in our experiment, two infrared heaters were suspended in parallel above the ground in order to, first, guarantee that sufficient experimental area would be warmed, secondly, to improve the uniformity of infrared heating, and thirdly, to avoid overheating in the centre (Kimball, 2005). Similar designs of multiple infrared heaters have previously been employed for warming experiments in other ecosystems (Duan et al., 2022; Roy et al., 2004).

Our results also showed that the soil volumetric moisture was marginally enhanced by warming during the growing season (Figure 6). This result is inconsistent with some of the previous studies in other ecosystems which showed that warming reduced soil moisture (Li et al., 2019; Wang et al., 2012; Wang, Quan, et al., 2021). Our result of increased moisture, which happened mainly during the period of soil thawing, occurred likely because warming led to an earlier thawing (and therefore wetting) of the soil (Figures 6 and 7). Warming-induced soil thawing and wetting, in line with our results, has also been observed in other permafrost regions, implying that changes in soil energy partitioning may indirectly cause the increases in soil moisture (Li et al., 2017; Natali et al., 2011). After soil thawing in ambient conditions, warming had nearly no significant effect on the soil moisture of the thawed soil, especially at the surface (Figure 6). Such response in soil moisture is probably because of the inherently high levels of soil moisture in the swamp meadow ($51.2 \pm 1.7\%$ for the surface soil

during the growing season at our study site), which might quickly replenish any losses caused by warming-enhanced evaporation (Peng et al., 2020). However, in the current whole-soil-profile and whole-ecosystem warming experiments worldwide, warming does significantly decrease soil moisture, especially in the surface soil (Hicks Pries et al., 2017; Malhotra et al., 2020). In these ecosystems, warming-induced soil drying mediated the responses of some crucial ecological processes (e.g. carbon input and carbon emission) to climate warming (Malhotra et al., 2020; Soong et al., 2021). A feature of the SWAMP experiment which should therefore be highlighted is that warming did not induce soil drying in this permafrost ecosystem, meaning that the direct effects of warming on the structure and functions of this ecosystem could be validly interpreted throughout this experiment.

Our results further demonstrated that soil thawing depth and the maximum thawing depth (i.e. active layer thickness) were deeper in the warmed plots than in the control plots during the growing season (Figure 7). These effects of the warming were in line with the primary objective of our experiment: to simulate an increase in active layer thickness. Based on the trends in active layer thickness over recent decades on the Tibetan Plateau (5–20 cm per decade; Peng et al., 2018; Wang et al., 2022; Xu & Wu, 2021), SWAMP is able to simulate the scenario of permafrost thawing in the next 10–20 years. This ability was also supported by the observed elevated temperature in the permafrost table (120 cm in the study site) by 0.6°C, which represented the warming in the next 10–20 years based on the trend over the last decade (0.48°C per decade; Cheng et al., 2019). Similar to CiPEHR in Alaska, USA, our experiment was able to simulate the deepening of active layer in permafrost ecosystems (Natali et al., 2011). Nevertheless, considering that the active layer thickness in the Tibetan alpine permafrost region was greater than that in the Arctic (e.g. ~230 cm on the Tibetan Plateau vs. ~50 cm in Alaska; Luo et al., 2016; Wang et al., 2022), it is hard to transmit heat from the surface to the permafrost using passive warming techniques (e.g. OTCs; Li et al., 2020; Wang & Wu, 2013). Subsequently, it is difficult to simulate permafrost warming in such regions with a thick active layer. Overcoming the aforementioned drawbacks, we have established the first experiment anywhere in the world to synchronously simulate permafrost warming and active layer deepening through the use of active warming techniques, and carried out a successful trial in Tibetan alpine permafrost region.

To summarize, the establishment of this *in situ* experiment represents a step towards more realistic simulation of future climate change in permafrost ecosystems, which will allow further exploration of the mechanisms underlying deep soil processes on active layer deepening. Along with this, some processes unique to permafrost ecosystems, rather than other types of ecosystems under the impact of climate warming, were also activated, by increasing soil thawing depth and prolonging thawing duration. As permafrost ecosystems are known for their extensive storage of soil carbon (Mishra et al., 2021), an increased active layer thickness would make more deep soil carbon accessible to soil microorganisms, which in turn may enhance the proportion of carbon released from deep soil

(Johnston et al., 2019; Miner et al., 2022). Meanwhile, thawing permafrost would release trapped nutrients (e.g. nitrogen), which would mitigate the nutrient limitation of plants and deep soil microbes, thus regulating the ecosystem carbon balance (Salmon et al., 2018; Zhang et al., 2023). These processes have not yet been fully quantified, which greatly constrains the ability of land surface models to accurately predict the potential permafrost C-climate feedback (Miner et al., 2022; Schuur et al., 2015). The establishment of the SWAMP experiment offers great potential to address these currently unresolved scientific questions, such as the responses of deep soil processes to permafrost thawing. Furthermore, the impact of climate warming on permafrost ecosystems are diverse and vary according to distinct mechanisms, histories and local conditions (Hicks Pries et al., 2015; Torn et al., 2015). With this in mind, we hereby call for more permafrost warming experiments, similar to this one, in other permafrost ecosystems worldwide (e.g. Siberia, Greenland and Alaska). Key parameters of the experiment, such as the plot size, the insertion depth of the heating rods and the warming duration, can be adjusted according to the conditions of the different permafrost ecosystems and the purpose of specific experimental designs. Recruiting further more permafrost warming experiments would provide a more robust approach for seeking more universal patterns of the permafrost ecosystem response to climate warming.

AUTHOR CONTRIBUTIONS

Yuanhe Yang, Yunfeng Peng, Yuxuan Bai and Guibiao Yang designed the research. Yuxuan Bai, Wei Zhou, Yuhong Xie and Qinlu Li performed the experiments. Yuxuan Bai and Yuanhe Yang led the writing, and Yunfeng Peng, Leiyi Chen and Biao Zhu participated in the writing. All authors have provided suggestions for revisions to the manuscript.

ACKNOWLEDGEMENTS

We thank the associate editor and two anonymous reviewers for providing valuable comments on the initial version of the manuscript. We are grateful to Yang Liu, Bin Wei and Guanqin Wang for their contributions to the experiment construction and to other members of Dr. Yuanhe Yang's research group for their contributions to improving the experimental design. We also thank Drs. Yunting Fang, Dongwei Liu from the Institute of Applied Ecology, Chinese Academy of Sciences and Dr. Ying Chen from Peking University for their suggestions on the warming system. This work was supported by the National Key Research and Development Program of China (2022YFF0801902) and the National Natural Science Foundation of China (31988102, 31825006, 32201405 and 32241034).

CONFLICT OF INTEREST STATEMENT

The authors declare no conflict of interest.

PEER REVIEW

The peer review history for this article is available at <https://www.webofscience.com/api/gateway/wos/peer-review/10.1111/2041-210X.14124>.

DATA AVAILABILITY STATEMENT

Data are available via the Dryad Digital Repository: <https://doi.org/10.5061/dryad.59zw3r2cd> (Bai et al., 2023).

ORCID

- Yuxuan Bai  <https://orcid.org/0000-0003-3451-2955>
Yunfeng Peng  <https://orcid.org/0000-0002-4151-4206>
Leiyi Chen  <https://orcid.org/0000-0002-3241-4676>
Biao Zhu  <https://orcid.org/0000-0001-9858-7943>
Yuanhe Yang  <https://orcid.org/0000-0002-5399-4606>

REFERENCES

- Bai, Y., Peng, Y., Zhou, W., Xie, Y., Li, Q., Yang, G., Chen, L., Zhu, B., & Yang, Y. (2023). Data from: SWAMP: A new experiment for simulating permafrost warming and active layer deepening on the Tibetan Plateau. *Dryad Digital Repository* <https://doi.org/10.5061/dryad.59zw3r2cd>
- Beermann, F., Langer, M., Wetterich, S., Strauss, J., Boike, J., Fiencke, C., Schirrmeyer, L., Pfeiffer, E. M., & Kutzbach, L. (2017). Permafrost thaw and liberation of inorganic nitrogen in eastern Siberia. *Permafrost and Periglacial Processes*, 28, 605–618. <https://doi.org/10.1002/ppp.1958>
- Benjamini, Y., & Hochberg, Y. (1995). Controlling the false discovery rate: A practical and powerful approach to multiple testing. *Journal of the Royal Statistical Society: Series B (Methodological)*, 57, 289–300. <https://doi.org/10.1111/j.2517-6161.1995.tb02031.x>
- Biskaborn, B. K., Smith, S. L., Noetzli, J., Matthes, H., Vieira, G., Streletskiy, D. A., Schoeneich, P., Romanovsky, V. E., Lewkowicz, A. G., Abramov, A., Allard, M., Boike, J., Cable, W. L., Christiansen, H. H., Delaloye, R., Diekmann, B., Drozdov, D., Etzelmüller, B., Grosse, G., ... Lantuit, H. (2019). Permafrost is warming at a global scale. *Nature Communications*, 10, 264. <https://doi.org/10.1038/s41467-018-08240-4>
- Chen, L., Liang, J., Qin, S., Liu, L., Fang, K., Xu, Y., Ding, J., Li, F., Luo, Y., & Yang, Y. (2016). Determinants of carbon release from the active layer and permafrost deposits on the Tibetan Plateau. *Nature Communications*, 7, 13046. <https://doi.org/10.1038/ncomms13046>
- Cheng, G., Zhao, L., Li, R., Wu, X., Sheng, Y., Hu, G., et al. (2019). Characteristic, changes and impacts of permafrost on Qinghai-Tibet plateau. *Chinese Science Bulletin*, 64, 2783–2795. <https://doi.org/10.1360/TB-2019-0191>
- Ding, J., Li, F., Yang, G., Chen, L., Zhang, B., Liu, L., Fang, K., Qin, S., Chen, Y., Peng, Y., Ji, C., He, H., Smith, P., & Yang, Y. (2016). The permafrost carbon inventory on the Tibetan Plateau: A new evaluation using deep sediment cores. *Global Change Biology*, 22, 2688–2701. <https://doi.org/10.1111/gcb.13257>
- Duan, Y., Liu, D., Huang, K., Shou, W., Zhu, F., Liu, Y., Yu, H., Gundersen, P., Kang, R., Wang, A., Han, S., Wang, Z., Zhu, J., Zhu, W., & Fang, Y. (2022). Design and performance of an ecosystem-scale forest soil warming experiment with infrared heater arrays. *Methods in Ecology and Evolution*, 13, 2065–2077. <https://doi.org/10.1111/2041-210X.13932>
- French, H., & Shur, Y. (2010). The principles of cryostratigraphy. *Earth-Science Reviews*, 101, 190–206. <https://doi.org/10.1016/j.earscirev.2010.04.002>
- Hallsworth, D. H., & Rouse, W. R. (1987). Soil heat flux in permafrost: Characteristics and accuracy of measurement. *Journal of Climatology*, 7, 571–584. <https://doi.org/10.1002/joc.3370070605>
- Hanson, P. J., Childs, K. W., Wullschleger, S. D., Riggs, J. S., Thomas, W. K., Todd, D. E., & Warren, J. M. (2011). A method for experimental heating of intact soil profiles for application to climate change experiments. *Global Change Biology*, 17, 1083–1096. <https://doi.org/10.1111/j.1365-2486.2010.02221.x>
- Hanson, P. J., Riggs, J. S., Nettles, W. R., Phillips, J. R., Krassovski, M. B., Hook, L. A., Gu, L., Richardson, A. D., Aubrecht, D. M., Ricciuti, D. M., Warren, J. M., & Barbier, C. (2017). Attaining whole-ecosystem warming using air and deep-soil heating methods with an elevated CO₂ atmosphere. *Biogeosciences*, 14, 861–883. <https://doi.org/10.5194/bg-14-861-2017>
- Henry, G. H. R., & Molau, U. (1997). Tundra plants and climate change: The international tundra experiment (ITEX). *Global Change Biology*, 3, 1–9. <https://doi.org/10.1111/j.1365-2486.1997.gcb132.x>
- Hicks Pries, C. E., Castanha, C., Porras, R. C., & Torn, M. S. (2017). The whole-soil carbon flux in response to warming. *Science*, 355, 1420–1423. <https://doi.org/10.1126/science.aal1319>
- Hicks Pries, C. E., van Logtestijn, R. S. P., Schuur, E. A. G., Natali, S. M., Cornelissen, J. H. C., Aerts, R., & Dorrepaal, E. (2015). Decadal warming causes a consistent and persistent shift from heterotrophic to autotrophic respiration in contrasting permafrost ecosystems. *Global Change Biology*, 21, 4508–4519. <https://doi.org/10.1111/gcb.13032>
- Hu, G., Zhao, L., Li, R., Wu, X., Wu, T., Xie, C., Zhu, X., & Su, Y. (2019). Variations in soil temperature from 1980 to 2015 in permafrost regions on the Qinghai-Tibetan Plateau based on observed and reanalysis products. *Geoderma*, 337, 893–905. <https://doi.org/10.1016/j.geoderma.2018.10.044>
- Hugelius, G., & Kuhry, P. (2009). Landscape partitioning and environmental gradient analyses of soil organic carbon in a permafrost environment. *Global Biogeochemical Cycles*, 23, GB3006. <https://doi.org/10.1029/2008GB003419>
- Jin, H., Luo, D., Wang, S., Lü, L., & Wu, J. (2011). Spatiotemporal variability of permafrost degradation on the Qinghai-Tibet Plateau. *Sciences in Cold and Arid Regions*, 3, 281–305. <https://doi.org/10.3724/SP.J.1226.2011.00281>
- Johnston, E. R., Hatt, J. K., He, Z., Wu, L., Guo, X., Luo, Y., Schuur, E. A. G., Tiedje, J. M., Zhou, J., & Konstantinidis, K. T. (2019). Responses of tundra soil microbial communities to half a decade of experimental warming at two critical depths. *Proceedings of the National Academy of Sciences of the United States of America*, 116, 15096–15105. <https://doi.org/10.1073/pnas.1901307116>
- Kimball, B. A. (2005). Theory and performance of an infrared heater for ecosystem warming. *Global Change Biology*, 11, 2041–2056. <https://doi.org/10.1111/j.1365-2486.2005.1028.x>
- Kimball, B. A., Alonso-Rodríguez, A. M., Cavalieri, M. A., Reed, S. C., González, G., & Wood, T. E. (2018). Infrared heater system for warming tropical forest understory plants and soils. *Ecology and Evolution*, 8, 1932–1944. <https://doi.org/10.1002/ece3.3780>
- Koven, C. D., Lawrence, D. M., & Riley, W. J. (2015). Permafrost carbon-climate feedback is sensitive to deep soil carbon decomposability but not deep soil nitrogen dynamics. *Proceedings of the National Academy of Sciences of the United States of America*, 112, 3752–3757. <https://doi.org/10.1073/pnas.1415123112>
- Kuang, X., & Jiao, J. (2016). Review on climate change on the Tibetan Plateau during the last half century. *Journal of Geophysical Research: Atmospheres*, 121, 3979–4007. <https://doi.org/10.1002/2015JD024728>
- Kuznetsova, A., Brockhoff, P. B., & Christensen, R. H. B. (2017). *lmerTest* package: Tests in linear mixed effects models. *Journal of Statistical Software*, 82, 1–26. <https://doi.org/10.18637/jss.v082.i13>
- Li, F., Peng, Y., Chen, L., Yang, G., Abbott, B. W., Zhang, D., Fang, K., Wang, G., Wang, J., Yu, J., Liu, L., Zhang, Q., Chen, K., Mohammat, A., & Yang, Y. (2020). Warming alters surface soil organic matter composition despite unchanged carbon stocks in a Tibetan permafrost ecosystem. *Functional Ecology*, 34, 911–922. <https://doi.org/10.1111/1365-2435.13489>
- Li, F., Peng, Y., Natali, S. M., Chen, K., Han, T., Yang, G., Ding, J., Zhang, D., Wang, G., Wang, J., Yu, J., Liu, F., & Yang, Y. (2017). Warming effects on permafrost ecosystem carbon fluxes associated with plant nutrients. *Ecology*, 98, 2851–2859. <https://doi.org/10.1002/ecy.1975>

- Li, F., Peng, Y., Zhang, D., Yang, G., Fang, K., Wang, G., Wang, J., Yu, J., Zhou, G., & Yang, Y. (2019). Leaf area rather than photosynthetic rate determines the response of ecosystem productivity to experimental warming in an alpine steppe. *Journal of Geophysical Research: Biogeosciences*, 124, 2277–2287. <https://doi.org/10.1029/2019JG005193>
- Li, Q., Liu, Y., Kou, D., Peng, Y., & Yang, Y. (2022). Substantial non-growing season carbon dioxide loss across Tibetan alpine permafrost region. *Global Change Biology*, 28, 5200–5210. <https://doi.org/10.1111/gcb.16315>
- Liu, G., Zhao, L., Li, R., Wu, T., Jiao, K., & Ping, C. (2017). Permafrost warming in the context of step-wise climate change in the Tien Shan Mountains, China. *Permafrost and Periglacial Processes*, 28, 130–139. <https://doi.org/10.1002/ppp.1885>
- Liu, H., Mi, Z., Lin, L., Wang, Y., Zhang, Z., Zhang, F., Wang, H., Liu, L., Zhu, B., Cao, G., Zhao, X., Sanders, N. J., Classen, A. T., Reich, P. B., & He, J. S. (2018). Shifting plant species composition in response to climate change stabilizes grassland primary production. *Proceedings of the National Academy of Sciences of the United States of America*, 115, 4051–4056. <https://doi.org/10.1073/pnas.1700299114>
- Luo, D., Wu, Q., Jin, H., Marchenko, S. S., Lü, L., & Gao, S. (2016). Recent changes in the active layer thickness across the northern hemisphere. *Environmental Earth Sciences*, 75, 555. <https://doi.org/10.1007/s12665-015-5229-2>
- Malhotra, A., Brice, D. J., Childs, J., Graham, J. D., Hobbie, E. A., Vander Stel, H., Feron, S. C., Hanson, P. J., & Iversen, C. M. (2020). Peatland warming strongly increases fine-root growth. *Proceedings of the National Academy of Sciences of the United States of America*, 117, 17627–17634. <https://doi.org/10.1073/pnas.2003361117>
- Marion, G. M., Henry, G. H. R., Freckman, D. W., Johnstone, J., Jones, G., Jones, M. H., Lévesque, E., Molau, U., Mølgaard, P., Parsons, A. N., Svoboda, J., & Virginia, R. A. (1997). Open-top designs for manipulating field temperature in high-latitude ecosystems. *Global Change Biology*, 3, 20–32. <https://doi.org/10.1111/j.1365-2486.1997.gcb136.x>
- McGuire, A. D., Lawrence, D. M., Koven, C., Clein, J. S., Burke, E., Chen, G., Jafarov, E., MacDougall, A. H., Marchenko, S., Nicolsky, D., Peng, S., Rinke, A., Ciais, P., Gouttevin, I., Hayes, D. J., Ji, D., Krinner, G., Moore, J. C., Romanovsky, V., ... Zhuang, Q. (2018). Dependence of the evolution of carbon dynamics in the northern permafrost region on the trajectory of climate change. *Proceedings of the National Academy of Sciences of the United States of America*, 115, 3882–3887. <https://doi.org/10.1073/pnas.1719903115>
- Miner, K. R., Turetsky, M. R., Malina, E., Bartsch, A., Tamminen, J., McGuire, A. D., Fix, A., Sweeney, C., Elder, C. D., & Miller, C. E. (2022). Permafrost carbon emissions in a changing Arctic. *Nature Reviews Earth & Environment*, 3, 55–67. <https://doi.org/10.1038/s43017-021-00230-3>
- Mishra, U., Hugelius, G., Shelef, E., Yang, Y., Strauss, J., Lupachev, A., Harden, J. W., Jastrow, J. D., Ping, C. L., Riley, W. J., Schuur, E. A. G., Matamala, R., Siewert, M., Nave, L. E., Koven, C. D., Fuchs, M., Palmtag, J., Kuhry, P., Treat, C. C., ... Orr, A. (2021). Spatial heterogeneity and environmental predictors of permafrost region soil organic carbon stocks. *Science Advances*, 7, eaaz5236. <https://doi.org/10.1126/sciadv.aaz5236>
- Natali, S. M., Schuur, E. A. G., Trucco, C., Hicks Pries, C. E., Crummer, K. G., & Baron Lopez, A. F. (2011). Effects of experimental warming of air, soil and permafrost on carbon balance in Alaskan tundra. *Global Change Biology*, 17, 1394–1407. <https://doi.org/10.1111/j.1365-2486.2010.02303.x>
- Nottingham, A. T., Meir, P., Velasquez, E., & Turner, B. L. (2020). Soil carbon loss by experimental warming in a tropical forest. *Nature*, 584, 234–237. <https://doi.org/10.1038/s41586-020-2566-4>
- Noyce, G. L., Kirwan, M. L., Rich, R. L., & Megonigal, J. P. (2019). Asynchronous nitrogen supply and demand produce nonlinear plant allocation responses to warming and elevated CO₂. *Proceedings of the National Academy of Sciences of the United States of America*, 116, 21623–21628. <https://doi.org/10.1073/pnas.1904990116>
- Obu, J., Westermann, S., Bartsch, A., Berdnikov, N., Christiansen, H. H., Dashstseren, A., Delaloye, R., Elberling, B., Etzelmüller, B., Kholodov, A., Khomutov, A., Kääb, A., Leibman, M. O., Lewkowicz, A. G., Panda, S. K., Romanovsky, V., Way, R. G., Westergaard-Nielsen, A., Wu, T., ... Zou, D. (2019). Northern hemisphere permafrost map based on TTOP modelling for 2000–2016 at 1 km² scale. *Earth-Science Reviews*, 193, 299–316. <https://doi.org/10.1016/j.earscirev.2019.04.023>
- Olefeldt, D., Goswami, S., Grosse, G., Hayes, D., Hugelius, G., Kuhry, P., McGuire, A. D., Romanovsky, V. E., Sannel, A. B. K., Schuur, E. A. G., & Turetsky, M. R. (2016). Circumpolar distribution and carbon storage of thermokarst landscapes. *Nature Communications*, 7, 13043. <https://doi.org/10.1038/ncomms13043>
- Peng, A., Klanderud, K., Wang, G., Zhang, L., Xiao, Y., & Yang, Y. (2020). Plant community responses to warming modified by soil moisture in the Tibetan Plateau. *Arctic, Antarctic, and Alpine Research*, 52, 60–69. <https://doi.org/10.1080/15230430.2020.1712875>
- Peng, X., Zhang, T., Frauenfeld, O. W., Wang, K., Luo, D., Cao, B., Su, H., Jin, H., & Wu, Q. (2018). Spatiotemporal changes in active layer thickness under contemporary and projected climate in the northern hemisphere. *Journal of Climate*, 31, 251–266. <https://doi.org/10.1175/JCLI-D-16-0721.1>
- Qin, W., Chen, Y., Wang, X., Zhao, H., Hou, Y., Zhang, Q., Guo, X., Zhang, Z., & Zhu, B. (2023). Whole-soil warming shifts species composition without affecting diversity, biomass and productivity of the plant community in an alpine meadow. *Fundamental Research*, 3, 160–169. <https://doi.org/10.1016/j.fmre.2022.09.025>
- R Core Team. (2022). *R: A language and environment for statistical computing*. R Foundation for Statistical Computing. <https://www.R-project.org/>
- Roy, B. A., Güsewell, S., & Harte, J. (2004). Response of plant pathogens and herbivores to a warming experiment. *Ecology*, 85, 2570–2581. <https://doi.org/10.1890/03-0182>
- Salmon, V. G., Schädel, C., Bracho, R., Pegoraro, E., Celis, G., Mauritz, M., Mack, M. C., & Schuur, E. A. G. (2018). Adding depth to our understanding of nitrogen dynamics in permafrost soils. *Journal of Geophysical Research: Biogeosciences*, 123, 2497–2512. <https://doi.org/10.1029/2018JG004518>
- Schuur, E. A. G., McGuire, A. D., Schädel, C., Grosse, G., Harden, J. W., Hayes, D. J., Hugelius, G., Koven, C. D., Kuhry, P., Lawrence, D. M., Natali, S. M., Olefeldt, D., Romanovsky, V. E., Schaefer, K., Turetsky, M. R., Treat, C. C., & Vonk, J. E. (2015). Climate change and the permafrost carbon feedback. *Nature*, 520, 171–179. <https://doi.org/10.1038/nature14338>
- Soong, J. L., Castanha, C., Hicks Pries, C. E., Ofiti, N., Porras, R. C., Riley, W. J., Schmidt, M. W. I., & Torn, M. S. (2021). Five years of whole-soil warming led to loss of subsoil carbon stocks and increased CO₂ efflux. *Science Advances*, 7, eabd1343. <https://doi.org/10.1126/sciadv.abd1343>
- Soong, J. L., Phillips, C. L., Ledna, C., Koven, C. D., & Torn, M. S. (2020). CMIP5 models predict rapid and deep soil warming over the 21st century. *Journal of Geophysical Research: Biogeosciences*, 125, e2019JG005266. <https://doi.org/10.1029/2019JG005266>
- Subcommitteee, P. (1988). Glossary of permafrost and related ground-ice terms. *Associate Committee on Geotechnical Research, National Research Council of Canada*, Ottawa, 156, 63–64.
- Torn, M. S., Chabbi, A., Crill, P., Hanson, P. J., Janssens, I. A., Luo, Y., Pries, C. H., Rumpel, C., Schmidt, M. W. I., Six, J., Schrumpf, M., & Zhu, B. (2015). A call for international soil experiment networks for studying, predicting, and managing global change impacts. *The Soil*, 1, 575–582. <https://doi.org/10.5194/soil-1-575-2015>
- Wang, D., Wu, T., Zhao, L., Mu, C., Li, R., Wei, X., Hu, G., Zou, D., Zhu, X., Chen, J., Hao, J., Ni, J., Li, X., Ma, W., Wen, A., Shang, C., La, Y., Ma, X., & Wu, X. (2021). A 1 km resolution soil organic carbon dataset

- for frozen ground in the third pole. *Earth System Science Data*, 13, 3453–3465. <https://doi.org/10.5194/essd-13-3453-2021>
- Wang, J., Quan, Q., Chen, W., Tian, D., Ciais, P., Crowther, T. W., Mack, M. C., Poulter, B., Tian, H., Luo, Y., Wen, X., Yu, G., & Niu, S. (2021). Increased CO₂ emissions surpass reductions of non-CO₂ emissions more under higher experimental warming in an alpine meadow. *Science of the Total Environment*, 769, 144559. <https://doi.org/10.1016/j.scitotenv.2020.144559>
- Wang, J., & Wu, Q. (2013). Impact of experimental warming on soil temperature and moisture of the shallow active layer of wet meadows on the Qinghai-Tibet Plateau. *Cold Regions Science and Technology*, 90–91, 1–8. <https://doi.org/10.1016/j.coldregions.2013.03.005>
- Wang, K., Zhang, T., Guo, H., & Wang, H. (2016). Climatology of the timing and duration of the near-surface soil freeze-thaw status across China. *Arctic, Antarctic, and Alpine Research*, 48, 723–738. <https://doi.org/10.1657/AAAR0016-009>
- Wang, S., Duan, J., Xu, G., Wang, Y., Zhang, Z., Rui, Y., Luo, C., Xu, B., Zhu, X., Chang, X., Cui, X., Niu, H., Zhao, X., & Wang, W. (2012). Effects of warming and grazing on soil N availability, species composition, and ANPP in an alpine meadow. *Ecology*, 93, 2365–2376. <https://doi.org/10.1890/11-1408.1>
- Wang, X., Ran, Y., Pang, G., Chen, D., Su, B., Chen, R., Li, X., Chen, H. W., Yang, M., Gou, X., Jorgenson, M. T., Aalto, J., Li, R., Peng, X., Wu, T., Clow, G. D., Wan, G., Wu, X., & Luo, D. (2022). Contrasting characteristics, changes, and linkages of permafrost between the Arctic and the third pole. *Earth-Science Reviews*, 230, 104042. <https://doi.org/10.1016/j.earscirev.2022.104042>
- Wu, Q., & Zhang, T. (2008). Recent permafrost warming on the Qinghai-Tibetan plateau. *Journal of Geophysical Research: Atmospheres*, 113, D13108. <https://doi.org/10.1029/2007JD009539>
- Xu, X., & Wu, Q. (2021). Active layer thickness variation on the Qinghai-Tibetan Plateau: Historical and projected trends. *Journal of Geophysical Research: Atmospheres*, 126, e2021JD034841. <https://doi.org/10.1029/2021JD034841>
- Xue, X., You, Q., Peng, F., Dong, S., & Duan, H. (2017). Experimental warming aggravates degradation-induced topsoil drought in alpine meadows of the Qinghai-Tibetan Plateau. *Land Degradation & Development*, 28, 2343–2353. <https://doi.org/10.1002/lrd.2763>
- Yadav, M., & Saxena, G. (1973). Effect of compaction and moisture content on specific heat and thermal capacity of soils. *Journal of the Indian Society of Soil Science*, 21, 129–132.
- Zhang, D., Wang, L., Qin, S., Kou, D., Wang, S., Zheng, Z., Peñuelas, J., & Yang, Y. (2023). Microbial nitrogen and phosphorus co-limitation across permafrost region. *Global Change Biology*. <https://doi.org/10.1111/gcb.16743>
- Zhang, G., Nan, Z., Hu, N., Yin, Z., Zhao, L., Cheng, G., & Mu, C. (2022). Qinghai-Tibet Plateau permafrost at risk in the late 21st century. *Earth's Future*, 10, e2022EF002652. <https://doi.org/10.1029/2022EF002652>
- Zhang, J., Wang, J., Chen, W., Li, B., & Zhao, K. (1988). *Vegetation of Xizang (Tibet)*. Science Press.
- Zhang, T., Barry, R. G., Knowles, K., Heginbottom, J. A., & Brown, J. (2008). Statistics and characteristics of permafrost and ground-ice distribution in the northern hemisphere. *Polar Geography*, 31, 47–68. <https://doi.org/10.1080/10889370802175895>
- Zhang, Z., Wu, Q., Jiang, G., Gao, S., Chen, J., & Liu, Y. (2020). Changes in the permafrost temperatures from 2003 to 2015 in the Qinghai-Tibet Plateau. *Cold Regions Science and Technology*, 169, 102904. <https://doi.org/10.1016/j.coldregions.2019.102904>
- Zou, D., Zhao, L., Sheng, Y., Chen, J., Hu, G., Wu, T., Wu, J., Xie, C., Wu, X., Pang, Q., Wang, W., Du, E., Li, W., Liu, G., Li, J., Qin, Y., Qiao, Y., Wang, Z., Shi, J., & Cheng, G. (2017). A new map of permafrost distribution on the Tibetan Plateau. *The Cryosphere*, 11, 2527–2542. <https://doi.org/10.5194/tc-11-2527-2017>

SUPPORTING INFORMATION

Additional supporting information can be found online in the Supporting Information section at the end of this article.

Appendix S1. Soil sampling and measurements.

Appendix S2. Pre-experiments for determining the insertion depth of heating rods.

Figure S1. Changes in mean annual soil temperature at different soil depths on the Tibetan Plateau from 1985 to 2015. Mean annual changes at 5 cm (a), 10 cm (b), 20 cm (c), and 40 cm (d). The solid line indicated the regression line, and the shade represented the 95% confidence interval. Totally, 10 sites containing weather station were selected with continuous measurements. Data were derived from the National Meteorological Information Center of China.

Figure S2. Changes in annual mean soil temperature at different depths in Tibetan alpine permafrost region between 1985 and 2015. The numbers on the right of the bar are the average values. Data from five sites with continuous observations were obtained from Hu et al. (2019).

Figure S3. Mean annual air temperature at the nearest weather station to the experimental site from 1959 to 2020. The solid line indicated the regression line, and the shade represented the 95% confidence interval. As the weather station at the study site was established in 2020 and no long-term monitoring data were recorded, the nearest weather station (~21 km; 37.34°N, 100.15°E) to the study site was chosen for presenting the long-term temperature dynamics. Data were derived from the National Meteorological Information Center of China.

Figure S4. Soil carbon content along the soil profile. Soil organic carbon (a), dissolved organic carbon (b), and soil inorganic carbon (c) content at various soil depths in plots that were set up as control and warmed before the start of experimental warming. More detailed statistical results can be seen in Table S3. Abbreviations: SOC, soil organic carbon; DOC, dissolved organic carbon; SIC, soil inorganic carbon. Significant level: ns, no significance; ***, p < 0.001.

Figure S5. Soil nitrogen content along the soil profile. Soil total nitrogen (a), dissolved inorganic nitrogen (b), NH₄⁺-N (c), and NO₃⁻-N (d) content at various soil depths in plots that were set up as control and warmed before the start of experimental warming. More detailed statistical results can be seen in Table S3. Abbreviations: TN, soil total nitrogen; DIN, dissolved inorganic nitrogen. Significant level: ns, no significance; ***, p < 0.001.

Figure S6. Soil physicochemical properties along the soil profile. Soil moisture (a) and pH (b) at various soil depths in plots that were set up as control and warmed before the start of experimental warming. Dashed line in panel (b) indicates neutral (pH = 7). More detailed statistical results can be seen in Table S3. Significant level: ns, no significance; ***, p < 0.001.

Figure S7. Design of the two pre-experiments at our study site. The left photograph in panel (a) showed the layout of the pre-experiments and formal experiment in the study site (a), and the right one

demonstrated the four treatments of the different insertion depths for heating rods. Panel (b) showed the diagram of the design for the second pre-experiment. The photograph in panel (a) was taken by W. Zhou in May 2021.

Figure S8. Soil temperature of the second pre-experiment at different depths from October 2020 to April 2021. Daily mean (\pm SE, $n=3$) soil temperature from 50 to 120 cm (a-g) and the mean differences in soil temperature at different depths (h-n) for treatments with heating rods being inserted at different depths during the non-growing season (from October 2020 to April 2021).

Figure S9. Realistic view of the two pre-experiments at our study site. Photographs of the first pre-experimental plots in May (a), June (b) and July (c) 2020, with heating rods being inserted at the permafrost table. The second pre-experimental plots with heating rods being inserted at different soil depths before the start of experimental warming (October 2020, d-f) and three months after the end of experimental warming (August 2021, g-i). Solid red lines in panel (g-i) indicate the collapse trends of the surface. Photographs in panel (a-c) were taken by Q. Li in May, June, and July 2020, separately. Photographs in panel (d-i) were taken by W. Zhou in May (d-f) and August (g-i) 2021.

Figure S10. Layout patterns for the heating rod in whole-soil-profile and whole-ecosystem warming experiments. Multi-loop heating rod layout in the SPRUCE experiment (Hanson et al. 2017; a).

Whole-soil-profile warming experiments used the layout with single-loop heating rod, and multi-loop heating cables in the surface (Hicks Pries et al. 2017; Qin et al. 2023; b). Ecosystem warming experiment in a salty marsh ecosystem arranged the heating rods in grid (Noyce et al. 2019; c). The 'loop + point' layout for the SWAMP experiment (d). **Table S1.** Information of the herbaceous species and their relative cover and height in the study site.

Table S2. Results of the linear mixed effect models on the effects of warming on air and soil temperature, soil moisture, and thawing duration during the growing season in 2022.

Table S3. Results of the linear mixed effect models on the effect of pre-warming setting and depth on soil carbon, nitrogen, and physicochemical characteristics before the start of experimental warming. Significant results are indicated in bold ($P<0.05$).

How to cite this article: Bai, Y., Peng, Y., Zhou, W., Xie, Y., Li, Q., Yang, G., Chen, L., Zhu, B., & Yang, Y. (2023). SWAMP: A new experiment for simulating permafrost warming and active layer deepening on the Tibetan Plateau. *Methods in Ecology and Evolution*, 14, 1732–1746. <https://doi.org/10.1111/2041-210X.14124>